Micrometer-Scale Ordering of Silicon-Containing Block Copolymer Thin Films via High-Temperature Thermal Treatments

Micrometer Scale Ordering of Silicon-Containing Block Copolymer Thin Films via High Temperature Thermal Treatments

Tommaso Jacopo Giammaria[1,2], Federico Ferrarese Lupi[1], Gabriele Seguini[1], Michele Perego[1]*, Francesco Vita[3], Oriano Francescangeli[3], Brandon Wenning[4], Christopher K. Ober[4], Katia Sparnacci[2], Diego Antonioli[2], Valentina Gianotti[2] and Michele Laus[2]**

[1] Laboratorio MDM, IMM-CNR, Via C. Olivetti 2, 20864 Agrate Brianza, Italy

[2] Dipartimento di Scienze e Innovazione Tecnologica (DISIT), Università del Piemonte Orientale ''A. Avogadro'', Viale T. Michel 11, 15121 Alessandria, Italy

[3] Dipartimento di Scienze e Ingegneria della Materia, dell'Ambiente ed Urbanistica and CNISM, Università Politecnica delle Marche, Via Brecce Bianche, 60131 Ancona, Italy

[4] Department of Materials Science and Engineering, Cornell University, Bard Hall, Ithaca, New York 14853, USA

KEYWORDS: high-χ block copolymer, self-assembly, thermal degradation, rapid thermal processing (RTP), surface functionalization

ABSTRACT

Block copolymers (BCPs) self-assembly is expected to complement conventional optical lithography for the fabrication of next generation microelectronic devices. In this regard, silicon-containing BCPs with a high Flory-Huggins interaction parameter (χ) are extremely appealing since they form high-resolution nanostructures with characteristic dimensions below 10 nm.

However, due to their slow self-assembly kinetics and low thermal stability, these silicon-containing high-χ BCPs are usually processed by solvent vapor annealing or in solvent rich ambient at low annealing temperature, significantly increasing the complexity of the facilities and of the procedures. In this work, the self-assembly of cylinder-forming polystyrene-*block*-poly(dimethylsiloxane-*random*-vinylmethylsiloxane) (PS-*b*-P(DMS-*r*-VMS)) BCP on flat substrates is promoted by means of a simple thermal treatment at high temperatures. Homogeneous PS-*b*-P(DMS-*r*-VMS) thin films covering the entire sample surface are obtained without any evidence of dewetting phenomena. The BCP arranges in a single layer of cylindrical P(DMS-*r*-VMS) nanostructures parallel oriented with respect to the substrate. By properly adjusting the surface functionalization, the heating rate, the annealing temperature, and the processing time, correlation length values larger than 1 μm are obtained in a timescale fully compatible with the stringent requirements of the microelectronic industry.

INTRODUCTION

Over the last decade, the aggressive scaling down of microelectronic devices forced the semiconductor industry to investigate novel manufacturing methods. Traditional "top-down" photolithographic processes are well established, extremely reliable and highly optimized, but have become prohibitively expensive to fabricate sub-20 nm structures.[1] Consequently, implementation of non-optical "bottom-up" lithographic approaches, based on self-organizing materials,[2,3] has been proposed to circumvent this problem. In particular, self-assembling block copolymers (BCPs) have become the subject of an intense research activity due to their ability to build up periodic sub-20 nm structures with a high degree of reproducibility and regularity.[4,5]

Polystyrene-*block*-polymethylmethacrylate (PS-*b*-PMMA) has been the work-horse in the field, providing a BCP-based technology platform for nanopatterning that can be easily integrated into standard fabrication processes of microelectronic industry.[6] Unfortunately, the relatively low Flory-Huggins interaction parameter χ (0.06 at 300 K)[7] limits the domain resolution of PS-*b*-PMMA to ca. 12 nm.[8,9] Silicon-containing BCPs are particularly promising to extend BCP lithography beyond PS-*b*-PMMA, since they commonly exhibit a χ value that is high enough to enable phase separation even at low degree of polymerization (N), with the formation of nanostructures below 10 nm. Moreover, during the removal of the organic block, the silicon-containing block can be oxidized to form a SiO_x structure, providing proper etch contrast for the subsequent pattern transfer into the substrate. In particular polystyrene-*block*-polydimethylsiloxane (PS-*b*-PDMS)[6,10] has attracted more and more interest, due to the very high Flory-Huggins interaction parameter (χ = 0.26 at 300 K)[11] and very small domain resolution.[12-14]

Unfortunately, the high incompatibility between the two blocks in silicon-containing BCPs inhibits the thermal diffusion of the polymeric chains and results in an extremely slow kinetic of the self-assembly and lateral ordering processes.[15] The self-assembly kinetic progressively slow down increasing the segregation strength (χN).[15] To speed up the process for a fixed N value, it would be highly desirable to thermally treat these BCPs at high temperatures. However the thermal stability of the silicon-containing block is expected to be relatively low with respect to the PS block,[16] limiting the processing temperature and, consequently, the mobility of the macromolecules during the thermally induced ordering. Accordingly, alternative polymer processing approaches, such as the so-called solvent vapor annealing (SVA), have been developed to promote the self-assembly in solvent rich ambients at low temperature, preventing the thermal degradation of the silicon-containing block.[17,18]

In the SVA process, the sample is exposed to solvent vapor at room temperature to reduce the glass transition temperature and to increase the mobility of the polymeric chains.[12,13,19] A significant enhancement of the lateral order in flat PS-*b*-PDMS thin films was observed by increasing annealing temperature and/or time during the SVA process.[20] Similarly, microwave-assisted SVA was proposed to further speed up the self-assembly process and to achieve a reasonable level of lateral order in the polymeric film.[21,22] More recently, the dewetting property of a polyvinyl alcohol (PVA) top-coat was exploited[23] to drive the self-assembly process and to obtain highly ordered structures in PS-*b*-PDMS thin films thermally treated at different temperatures for approximately two hours. These solvent assisted approaches require the implementation of complex experimental setups and protocols that prevent a fine-tuning of the processing parameters (vapor pressure, chamber temperature, etc.), often resulting in a poor reproducibility of the experimental results. For this reason, their effective integration in a

production process flow is not clear-cut. In this regard, a simple thermal treatment to promote the BCP self-assembly in few minutes would be highly desirable.

Park *et al.*[19] obtained poorly ordered sub-10 nm cylindrical nanostructures in PS-*b*-PDMS thin films confined within topographically defined trenches by means of a pure thermal treatment performed at 200 °C for 300 s in oven under vacuum. However, the formation of highly defective self-assembled BCP films were reported when processing the samples at temperatures above 200 °C. Aissou *et al.*[24] reported the self-assembly and perpendicular orientation of silicon-containing BCP thin films within a guiding pattern by thermal treatments at 100 °C and 180 °C for 600 s. Very recently Seshimoto *et al.*[25] obtained perpendicular oriented sub-10 nm silicon-containing BCP lamellae on flat surfaces, by atmospheric thermal annealing at 130 °C for only 1 min. They observed the formation of terrace structures increasing the annealing temperature at 140 °C. Annealing the BCP films at 150 °C no periodic structures were detected due to a drastic variation in the orientation of the BCP microdomains. Interestingly in all these articles, the self-assembly of the silicon-containing BCPs was achieved at annealing temperatures equal or below 200°C. Moreover no quantitative measurements of the lateral order in the self-assembled silicon-containing BCP thin films were reported. Even more important no data are available about the self-assembly of these silicon-containing macromolecules at high temperatures.

The present work investigates the self-assembly and ordering process in cylinder-forming polystyrene-*block*-poly(dimethylsiloxane-*random*-vinylmethylsiloxane) (PS-*b*-P(DMS-*r*-VMS)) during high temperature thermal treatments. Figure 1 shows the chemical structure of the BCP under investigation. Proper substrate functionalization has been established to assure a uniform coverage of the substrate, avoiding any dewetting of the PS-*b*-P(DMS-*r*-VMS) thin films. The correlation length ξ in the self-assembled polymeric films has been measured to quantitatively

assess the lateral order in the different BCP samples. In particular the evolution of the correlation length ξ has been explored as a function of substrate functionalization, annealing temperature (T_a) and time (t_a). A viable solution for the processing of this high-χ BCP has been identified.

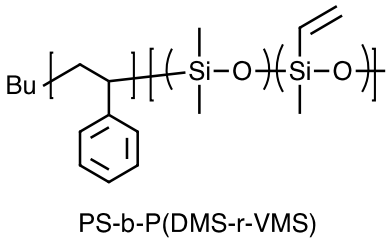

PS-b-P(DMS-r-VMS)

Figure 1. Chemical structure of PS-*b*-P(DMS-*r*-VMS).

EXPERIMENTAL

Materials

2-hydroxyethyl(2-bromoisobutyrate) (HEBIB), tris(2-(dimethylamino)ethyl)amine (Me6TREN), copper(II) bromide ($CuBr_2$), tin(II) 2-ethylhexanoate ($Sn(EH)_2$), hexamethylcyclotrisiloxane (D3), 1,3,5-trivinyl-1,3,5-trimethylcyclotrisiloxane (V3), n-butyl lithium, sec-butyl lithium, sodium metal, calcium hydride (CaH_2), diphenylethylene, styrene (S), methylmethacrilate (MMA), tetrahydrofuran (THF), benzene and anisole were purchased from Aldrich. MMA was purified by passing through an inhibitor removal column (Aldrich) before use. Benzene was dried by stirring over n-butyl lithium and diphenylethylene and distilled, then degassed by a freeze pump thaw process. THF was dried by stirring over sodium metal and benzophenone, distilled and degassed by a freeze pump thaw process. S was dried by stirring over ground CaH_2, then distilled and degassed by a freeze pump thaw process. D3 was dried by stirring in benzene over CaH_2. After drying, the benzene was distilled and D3 sublimed into a flask containing benzene and dried S polymerized with sec-butyl lithium. D3 was stirred at room temperature

over the polymerization to further dry until the solution was clear, then the benzene was distilled and D3 sublimed into a clean flask. V3 was dried by stirring over CaH_2 at 40 °C, then distilled and degassed by a freeze pump thaw process.

The macromonomer mono(methacryloxypropyl)-terminated polydimethylsiloxane (MPDMS) (viscosity 10 cSt, Mn 800 g mol^{-1}) was purchased from ABCR GmbH and used as received. α-hydroxyl ω-Br polystyrene (PS) and α-hydroxyl ω-Br polymethylmethacrylate (PMMA) homopolymers as well as two α-hydroxyl ω-Br P(S-*r*-MMA) RCPs with S units percent of 58% and 62%, marked R58 and R62 respectively, were synthesized by ARGET ATRP[26,27] copolymerization of Styrene (S) and methylmethacrylate (MMA). The PS-*b*-P(DMS-*r*-VMS) BCP and the α-hydroxyl ω-Br P(S-*r*-MPDMS) RCP, were synthesized as described in the following section. The structures of the macromonomer MPDMS and of the corresponding α-hydroxyl ω-Br P(S-*r*-MPDMS) RCP are reported in Figure 2.

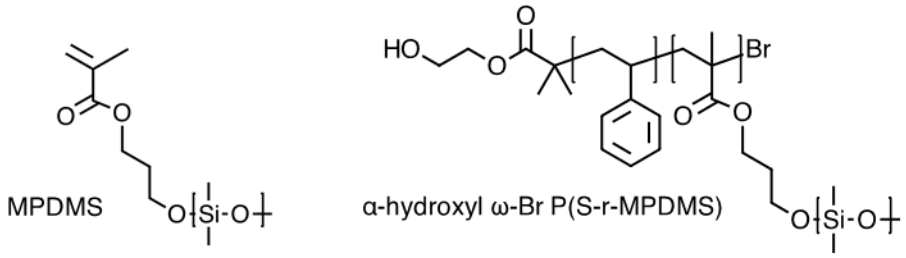

Figure 2. Chemical structure of the macromonomer MPDMS and the α-hydroxyl ω-Br P(S-*r*-MPDMS).

Synthesis of PS-b-P(DMS-r-VMS) block copolymer

A clean dry flask evacuated with nitrogen was filled with 50 mL of dried benzene. To this, 487 µL of 1.4 M sec-butyl lithium in hexane were added and stirred, followed by the addition of 12 mL of dried S. The polymerization of S was run for 24 h to consume all the monomer in the solution and a sample was taken after 24 h for analysis by SEC. A 0.5 g mL^{-1} solution of D3 in

dried benzene was prepared to add to the polymerization. 5.8 mL of this solution (2.9 g of D3) were added to the polymerization to initiate the D3 polymerization. This was allowed to react for 24 h until the solution was colorless. At this time, 18 mL of distilled THF were added to the reaction to accelerate the polymerization of the D3. After 6 h, 1.25 mL of V3 was added to the polymerization and reacted at room temperature for 5 additional days. To terminate the polymerization, 0.5 mL of degassed methanol was added to the polymerization and allowed to stir for 15 minutes to terminate the polymerization. The polymer was precipitated by stirring in 1 L of methanol, filtered and dried. The polymer was characterized by SEC to determine final molecular weight, and by NMR to determine vinyl content. The vinyl content of the siloxane block was determined to be 29.9%. The PS and PS-*b*-P(DMS-*r*-VMS) were run through SEC to determine molecular weight. The PS was 15800 g mol^{-1} with a PDI of 1.02 and the PS-*b*-P(DMS-*r*-VMS) was 22000 g mol^{-1} with a PDI of 1.03, giving a total siloxane molecular weight of 6200 g mol^{-1}.

Synthesis of P(S-r-MPDMS) random copolymer

The functional RCP P(S-*r*-MPDMS) was obtained by ARGET ATRP copolymerization[26,27] of S and MPDMS initiated by HEBIB and catalyzed by $CuBr_2$/Me_6TREN complex in the presence of $Sn(EH)_2$ as the reducing agent. In detail, 1.35 mg $CuBr_2$ (6.02 μmol) and 1.6 μL Me_6TREN (6.02 μmol) were dissolved in 3.5 mL degassed anisole, and transferred via degassed syringes to a dry Schlenk flask, purged by flushing with nitrogen. Then, 5.0 mL degassed S (43.7 μmol), 2.0 ml degassed PDMSMA (25.7 mmol) and 45.0 μL HEBIB (0.31 mmol) were added and the mixture was degassed by three freeze-thaw cycles. Next, a purged solution of $Sn(EH)_2$ (60.2 μmol) and Me_6TREN (60.2 μmol) in degassed anisole (1.0 mL) was added and the mixture was sealed

under nitrogen. The polymerization was carried out at 90 °C for 22 h. Then, the reaction mixture was cooled to room temperature and the copolymer was precipitated into cold methanol, washed with cold methanol, purified by precipitation from THF solution into cold methanol, and then dried under vacuum at room temperature. The monomer conversion was 55 % (w_t/w_t) as determined gravimetrically.

Polymer characterization

The molar mass data were determined by SEC analysis, performed on THF solutions using a 590 Waters chromatograph equipped with refractive index and ultraviolet detectors and using a column set consisting of Waters HSPgel HR3 and HR4 with a flow rate of 0.6 mL min^{-1}. The column set was calibrated against standard PS samples.

Thermal treatments

All the thermal treatments described in the following were performed in a Jipelec JetFirst Series RTP machine. The heating rate was set to 18 °C s^{-1}. The temperature of the sample is constantly monitored in real time by a thermocouple place underneath the sample. All the treatments were performed in ultra-pure nitrogen. The grafting process of the hydroxyl-terminated homo and copolymers was performed at 250 °C for 600 s, whereas the BCP self-assembly was promoted by RTP annealing at temperatures comprised between 190 °C and 350 °C for times ranging from 1 s to 900 s, according to the procedure reported elsewhere.[28]

Substrate preparation

Seven substrates were prepared and tested. Two hard surfaces, corresponding to as received and piranha treated SiO_2 substrate with ~2 nm thick native SiO_2 layer were employed. The piranha solution (H_2SO_4/H_2O_2 with 1/3 v/v ratio) was applied at 80 °C for 40 minutes in order to eliminate any residual organic materials and increase the hydroxyl groups density onto the SiO_2 surface. The samples were then rinsed in H_2O, subsequently in 2-propanol and finally dried under N_2 flow. Five soft surfaces were prepared by grafting two α-hydroxyl ω-Br homopolymers namely a functional polystyrene (PS) and a polymethylmethacrylate (PMMA) as well as two functional poly(styrene-*r*-methylmethacrylate) RCPs with S unit percentages of 58 (R58) and 62% (R62) and a P(S-*r*-MPDMS) RCP.

In details, solutions of R58, R62, P(S-*r*-MPDMS), PS, and PMMA (18.0 mg in 2.0 mL of toluene) were prepared and sonicated in ultrasonic bath for 300 s. The solutions obtained were then spun on the substrates at 3000 rpm for 30 s. Samples were thermally treated in RTP at 250 °C for 600 s in order to promote the grafting reaction of the hydroxyl-functionalized polymers with the silanol groups of the SiO_2 substrate. After annealing the non-grafted polymers chains were removed by means of sonication of the samples in ultrasonic bath in toluene. The thickness of the resulting polymer brush layers were measured by ellissometry.

PS-b-P(DMS-r-VMS) self-assembly condition

A solution of PS-*b*-P(DMS-*r*-VMS) (18.0 mg in 2.0 mL of toluene) was prepared, sonicated in an ultrasonic bath, and finally spun (3000 rpm, 30 s) on the different substrates. The BCP solution concentration were optimized in order to obtain polymeric films with thickness around 25 nm. The self-assembly of the cylindrical nanostructures was achieved by means of a simple thermal treatment in a RTP machine (Jipelec, JetFirst Series system).

Thin film characterization

The thicknesses of the polymer brushes and of the PS-*b*-P(DMS-*r*-VMS) films were measured by means of a M-200U spectroscopy ellipsometer (J.A. Wallom Co., Inc.) using a Xenon lamp at 70° incident angle.

The roughness of the polymer brushes was determined starting from AFM images acquired in tapping mode using a Dimension Edge instrument (Bruker) equipped with a topography probe (PPP-NCHR, Nanosensors).

The WCAs of the SiO_2 substrates and of the different brush layers were measured using an optical tensiometer Attension mod. Theta.

Scanning Electron Microscopy analysis (SEM)

A Zeiss Supra 40 SEM was utilized to evaluate the morphology and the nanostructures of the samples. Reactive Ion Etching (RIE) treatment was used to remove the upper PDMS layer formed during the self-assembly of the PS-*b*-P(DMS-*r*-VMS) thin films. The process was performed in a Plasmalab 80 Plus system. The power of the RF generator was set at 120W and the bias voltage at 340 V. A mixture of CHF3 (60 sccm) and Ar (25 sccm) at a pressure of 40 mTorr, for 20 s was used. Finally, an O_2 Plasma treatment at 40 W for 60 s was performed to remove the PS component of the matrix and oxidize the PDMS increasing the contrast for the subsequent analysis. The calculation of the correlation length (ξ) was done by processing several high resolution SEM images with dimension of 16.2 µm x 11.2 µm with Matlab routine following the procedure described in refs[29,30]. As a result a directional map of the entire SEM image is visualized by applying a color scale to each angular information in the range from 0 to

180°. In figure S1 a representative color map is merged with the corresponding SEM image in order to further elucidate the output of the computational procedure. The lateral order of the cylindrical nanostructures parallel oriented with respect to the substrate was determined by extracting the correlation length (ξ) values from the color maps. The mean values of ξ and the corresponding standard deviations were calculated taking more than five SEM images from different regions for each sample.

Grazing-Incidence Small-Angle X-ray Scattering (GISAXS) measurements

GISAXS measurements were performed at the BM32 beamline of the European Synchrotron Radiation Facility (ESRF, France), using a 7 KeV beam energy (wavelength $\lambda = 0.177$ nm) and a two-dimensional CCD detector (Photonic Science ImageStar 9000) set at a distance of 1.348 m from the sample. The detector was orthogonal to the incident X-ray beam, while the sample was mounted on a high-resolution goniometer, allowing a fine control of the incidence angle. A vacuum chamber was placed between the sample and the detector to minimize X-ray scattering from air.

TGA-GC-MS analysis

The TGA-GC-MS analyses were performed using a Mettler TGA/SDTA 851e purged with a steady flow of inert gas at a scanning rate of 20 °C min^{-1} from room temperature to 1100 °C. For bulk materials, each sample was placed in an open alumina crucible. The GC-MS analysis was performed using a FINNIGAN TRACE GC-ULTRA and TRACE DSQ. The GC separation was carried out using a Phenomenex DB5-5ms capillary column (30 m, 0.25 i.d., 0.25 thickness). The

injector temperature was set at 250 °C in splitless mode and helium was used as carrier gas at a constant flow of 1.0 mL min^{-1}. The MS transfer line and the oven temperatures were set at 270 °C and 150 °C, respectively.

The evolved gas from TGA was transferred to the GC-MS using the interface described elsewhere.[31] The transfer lines from the TGA to the interface and from the interface to the GC were set at the temperature of 200 °C, the temperature of the interface was 150 °C and the sampling frequency was 30 s^{-1}. The sampled gas from the loop to the waste was switched after 10 s and the capacity of the injection loop was 2.5 mL. The MS signal was acquired in EI+ mode with ionization energy of 70.0 eV and at the ion source temperature of 250 °C. The acquisition was performed both in full-scan mode, in the 20–350 *m/z* range and in Single Ion Monitoring (SIM) mode by acquiring the signals corresponding to styrene (S) at 104 *m/z*, methylmethacrylate (MMA) at 100 m/z and hexamethyltriciclosiloxane (HMTCS) at 207 *m/z*.

Direct Exposure Probe analysis

The PS-*b*-P(DMS-*r*-VMS) BCP and the α-hydroxyl ω-Br PMMA homopolymer were subjected to a direct mass spectrometric analysis by a direct exposure probe (DEP) tool (Thermo Electron Corporation) that permits a rapid heating of the sample deposited on a thin filament. The DEP probe is hyphenated with a quadrupolar mass spectrometer (Finnigan TRACE DSQ). The filament was a wire of Rhenium with a loop at the end inserted in a ceramic base. The filament temperature was regulated by properly adjusting the electric current flowing in the filament. A solution was prepared by dissolving the relevant copolymer (2.0 mg) in dichloromethane (10.00 mL). A single drop of 3 μL of this solution was deposited on the filament using a calibrated microsyringe of 10 μL in volume. Then, the solvent was eliminated by heating the filament for

60 s at 50 °C. Several thermal treatments were performed imposing different heating rates, namely 1, 10, 20, 50, and 100 °C s^{-1} starting from 25 °C to reach 700 °C. Mass spectrometric detection was performed in SIM mode acquiring the signals corresponding to S at 104 *m/z*, MMA at 100 *m/z*, and HMTCS at 207 *m/z* in EI+ mode (ionization energy = 70.0 eV) and at the ion source temperature of 250 °C.

RESULTS AND DISCUSSIONS

PS-b-P(DMS-r-VMS) thermal stability

To understand the effect of high temperature thermal treatments on PS-*b*-P(DMS-*r*-VMS) and identify an accessible processing window, the thermal stability of this silicon containing BCP was investigated in details. The degradation of PDMS homopolymer is known to occur by two separate mechanisms.[16] At relatively low temperatures and slow heating rate, the PDMS degradation proceeds via depolymerization of the polysiloxane backbone leading to formation of cyclosiloxanes. At higher temperatures and fast heating rate, the degradation of the PDMS occurs through a radical mechanism involving Si-CH_3 homolytic bond cleavage followed by hydrogen abstraction to form methane. On the other hand, the degradation of PS homopolymer[32,33] involves statistical chain breaking followed by a depropagation process which is the result of a competition between three different reaction mechanisms: unzipping, intramolecular and intermolecular hydrogen transfer. The typical pyrolysis products of PS are the styrene (S) monomer, the dimer, and the trimer, although the S monomer represents definitely the major product.

The bottom section of Figure 3 reports thermogravimetric analysis - gas chromatography - mass spectrometry (TGA-GC-MS) analysis of PS-*b*-P(DMS-*r*-VMS) in the bulk, from room

temperature to 900 °C, with a heating rate of 0.33 °C s^{-1}. This specific heating rate was selected to reproduce conventional operating conditions of standard furnaces. The bottom section of Figure 3 illustrates the TGA-GC-MS chromatograms with specific reference to mass peaks at 207 and 104 *m/z*, corresponding to the hexamethyltricyclosiloxane (HMTCS) and S, respectively. The occurrence of other siloxane oligomers was observed but their intensity was lower than that of HMTCS. Similarly, the signals corresponding to dimer or trimers of S are extremely low.

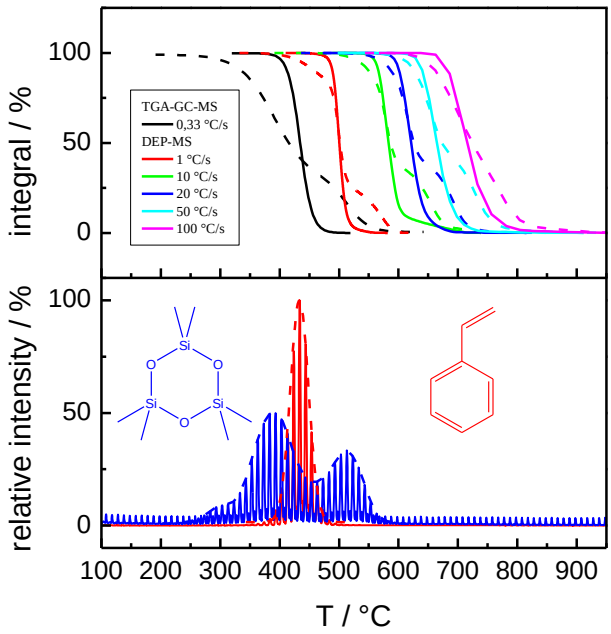

Figure 3. Top section, TGA-GC-MS integral curves of PS-*b*-P(DMS-*r*-VMS) and at *m/z* 207 (black dashed line) and 104 (black continuous line); Integral of DEP-MS signals for PS-*b*-P(DMS-*r*-VMS) at different heating rate with reference to mass peak at *m/z* 104 and at *m/z* 207, corresponding to S (continuous lines) and HMTCS (dashed lines), respectively. Bottom section, TGA-GC-MS chromatograms with reference to the mass peaks at *m/z* 207 (blue curve) and 104 (red curve) corresponding to HMTCS and S, respectively

According to these results, the effect of high temperature thermal treatments on the PS-*b*-P(DMS-*r*-VMS) can be sketched just considering the evolution of both S and HMTCS. The

sampling of the evolved gas occurred every 30 s and the dashed lines, joining the GC peaks, mark and contour the entire loss profiles. In the top section of the Figure 3, the integrals of the GC profiles (black lines) for both the evolved products are reported. The thermal evolutions of S and HMTCS are quite different. The S loss extends from 400 °C to 480 °C with a single peak at 430 °C whereas the HMTCS loss is rather broad, extending from 280 °C to 550 °C with two main losses at 380 °C and 500 °C.

These experimental data indicate that, consistently with literature reports on PDMS homopolymers,[16] The thermal stability of the P(DMS-*r*-VMS) block is significantly lower with respect to that of the PS block. Consequently, the P(DMS-*r*-VMS) block hampers the possibility to process the PS-*b*-P(DMS-*r*-VMS) system at temperatures higher than 300°C in the bulk phase. Nevertheless the thermal stability of macromolecules in the form of thin films is usually significantly higher than in the bulk.[31,34,35] Moreover, as reported by Deshpande *et al.*,[16] the onset of the thermal degradation of PDMS homopolymers critically depends on the processing conditions and moves toward high temperatures as processing is performed at high heating rates for short annealing time periods.[16] Consequently the possibility to extend the window of accessible temperatures for PS-*b*-P(DMS-*r*-VMS) thin film was explored by investigating the thermal stability of the BCP under dynamic conditions.

The top section of Figure 3 reports the Direct Exposure Probe (DEP) mass profiles (colored lines) of S and HMTCS for PS-*b*-P(DMS-*r*-VMS) thin films during thermal treatments performed at different heating rates ranging from 1 °C s^{-1} to 100 °C s^{-1}. The shapes of the loss curves in thin films are quite similar to the ones obtained in the bulk (black lines) but significantly shifted along the temperature scale. Moreover the degradation profiles in thin films are progressively shifted to higher values along the temperature scale as the heating rate

increases. In particular, when the heating rate is 20 °C s^{-1}, the beginning of the thermal degradation of the P(DMS-*r*-VMS) block occurs at approximately 500 °C. This experimental result indicates that, during thermal treatment with very fast heating rates, the onset of the degradation temperature moves toward higher values thus increasing the accessible temperature window for the processing of the PS-*b*-P(DMS-*r*-VMS) films. Consequently high temperature thermal treatments are expected to be possible on this specific silicon containing BCP, provided that the polymeric film is driven to the target temperature in a quite short time, in order to prevent the ignition of the degradation process in P(DMS-*r*-VMS) block.

Recently, we demonstrated that high temperature treatments in a rapid thermal processing (RTP) machine are suitable to promote long range ordering in symmetric and asymmetric PS-*b*-PMMA thin films, within a timescale compatible with the stringent requirement of the microelectronic industries.[28] Using this technology, the sample temperature can be driven well above the glass transition (T_g), stabilized at the desired ordering temperature and finally decreased below T_g in few seconds, thus preventing any significant degradation of the polymeric material.[26,36] In the following sections the possibility to drive the self assembly process in PS-*b*-P(DMS-*r*-VMS) thin films is explored in details using an RTP machine operating at high temperatures with a fixed heating rate of 20 °C s^{-1}.

Functionalization of SiO_2

The functionalization of SiO_2 surfaces with a polymeric brush layer has already been studied by several authors in order to achieve uniform coverage of the samples with different silicon containing BCP thin films.[37-40] To ensure the formation of uniform BCP thin films onto the substrate, we functionalized the substrates with brush layers having different chemical compositions in order to finely tune the surface energy of the substrates and minimize dewetting

phenomena during the processing of the specific silicon containing BCP under investigation,. In particular seven different substrates were prepared and tested. Two hard surfaces, corresponding to the as received SiO_2 substrate and the same substrate after the piranha treatment were considered as references. Soft surfaces with tethered polymeric brush layers were prepared by grafting α-hydroxyl ω-Br homopolymers and random copolymers (RCPs), having different chemical structure and composition.

Functional polystyrene (PS) and polymethylmethacrylate (PMMA) homopolymers as well as two functional poly(styrene-*random*-methyl methacrylate) P(S-*r*-MMA) RCPs with S unit percent of 58% (R58) and 62% (R62) and a poly(styrene-*random*-monomethacryloxypropylpolydimethylsiloxane) P(S-*r*-MPDMS) RCP with S unit percent of 70% were used, to systematically vary the surface energy of the substrate prior to PS-*b*-P(DMS-*r*-VMS) deposition. The molecular weight of the various functional homopolymers and RCPs was comprised between 11800 g mol^{-1} and 16000 g mol^{-1}, whereas polydispersity indexes (PDI) (M_w/M_n) ranging from 1.14 to 1.36 were obtained. The grafting of these functional polymers to the surface of SiO_2, after activation with the piranha solution, was performed by thermal annealing in RTP at 250 °C for 600 s.[41] The thicknesses and roughness of the different brushes as well as the corresponding water contact angles (WCAs) for all the substrates are reported in Table 1.

Table 1. Physical-chemical characterization of the variously treated SiO_2 substrates. WCAs, film thickness and roughness of the polymer brushes grafted to the SiO_2 substrate at T_a = 250 °C for t_a = 600 s. Film thickness of PS-*b*-P(DMS-*r*-VMS) thin films spin coated on the different substrates and treated at T_a = 230 °C for t_a = 300 s.

Substrate		Water contact angle (°)	Brush Thickness (nm)	Brush roughness (nm)	BCP Thickness (nm)
SiO_2	As received	63.5	/	/	24.8
	Piranha treated	8.4	/	/	25.8
Brush Layer	PMMA	69.0	7.8	0.45	24.0
	R58	79.0	8.0	0.23	26.4
	R62	80.0	8.1	0.23	25.6
	PS	92.0	9.3	0.23	22.2
	P(S-*r*-MPDMS)	104.5	7.0	0.26	25.3

Ellipsometric measurements indicate that the thicknesses of the different brush layers are quite similar for all the samples. The measured thickness values ranged from 7 nm to 9 nm, as expected considering their very similar molecular weight values.[42] Tapping mode AFM analysis reveals minimal variation of the brush layer roughness. Figure S2 shows representative topographic images of the different polymeric brushes. The measured root-mean-square roughness values of the brush layers range between 0.23 nm and 0.45 nm because of the low PDI index of the homopolymers and RCPs. These small roughness values reflect the uniform grafting of the OH-terminated polymers onto the SiO_2 substrates that produced very homogeneous and compact polymeric brush layers. The WCA of as received and piranha treated SiO_2 result 63.5° and 8.4°, respectively, indicating that the piranha treatment causes a significant increase in the surface hydrophilicity. The P(S-*r*-MPDMS) brush layer exhibits the highest WCA value (104.5°) while the PMMA brush corresponds to the lowest (69.0°). The PS brush layer has a contact angle of 92.0° and the values of R62 (79.6°) and R58 (79.0°) brushes are located between PS and PMMA brushes.

PS-b-P(DMS-r-VMS) thin film deposition and ordering

PS-*b*-P(DMS-*r*-VMS) thin films were spun on the different substrates. The experimental parameters were adjusted to obtain BCP layers with a thickness of approximately 25 nm. The effective thicknesses of the different BCP films were measured by ellipsometry and reported in Table 1. The samples were subsequently annealed in RTP at 230 °C for 300 s to promote self-assembly and lateral ordering of the nanodomains. Systematic scanning electron microscopy (SEM) and grazing-incidence small-angle X-ray scattering (GISAXS) analyses were performed on all the samples to determine the morphological parameters of the P(DMS-*r*-VMS) cylindrical nanostructures and evaluate the lateral order within the polymeric film. Figure S3 shows representative cross-sectional SEM images of the BCP film to highlight the cylindrical morphology. Representative SEM plan view images at low and high magnification are reported in Figure 4a and 4b, respectively.

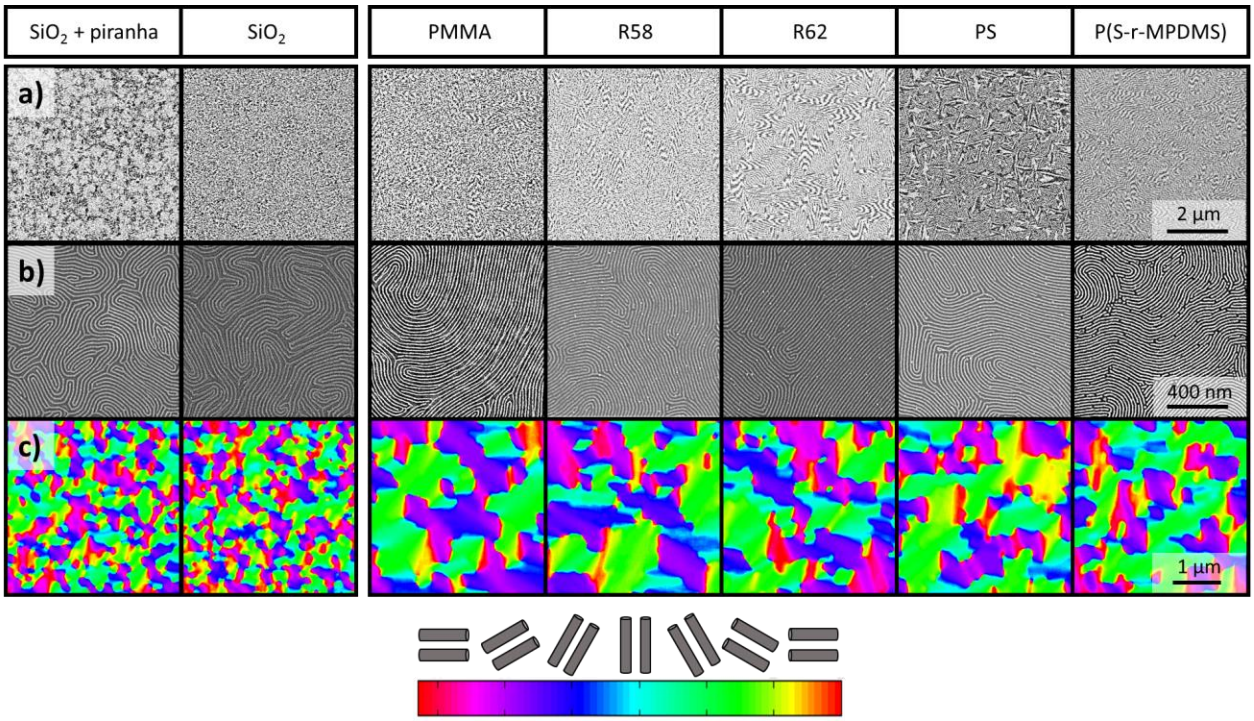

Figure 4. Low (a) and high (b) magnification SEM images of the PS-*b*-P(DMS-*r*-VMS) thin films deposited on different substrates after the ordering process at T_a = 230 °C for t_a = 300 s. The color maps (c), associated to the corresponding SEM images, delimiting the domain boundaries are also illustrated. The legend below the figure correlate the orientation of the cylinder in the SEM images with the color scale.

At low magnification, light and dark grey areas are visible in the PS-*b*-P(DMS-*r*-VMS) films deposited on the as received SiO_2 and on the piranha-treated SiO_2 substrates, thus indicating inhomogeneous coverage of the surface with the formation of disordered structures with perpendicular and in plane cylinders randomly distributed on the substrate, as showed in figure S4. In contrast, homogeneous coverage of the substrate with ordered grains structures, as indicated by the presence of Moiré patterns in the SEM images,[43] were observed in the PS-*b*-P(DMS-*r*-VMS) films deposited on the substrates modified with the functional homopolymers and RCPs. Therefore, the presence of a polymer brush layer is a requisite to achieve a uniform coverage of the substrate and to avoid non-homogeneities in the PS-*b*-P(DMS-*r*-VMS) thin films, in agreement with literature results.[38,44]

The characteristic dimensions of the PS-*b*-P(DMS-*r*-VMS) pattern can be investigated by analyzing the high magnification SEM images of Figure 4b. All the samples exhibit regular patterns with P(DMS-*r*-VMS) cylinders lying parallel to the substrate with diameter d = 9 ± 1 nm and lattice spacing L_0 = 20 ± 1 nm.

The domain coarsening as a function of the substrate functionalization is depicted in Figure 4c, in which the color maps delimiting the grain boundaries are located in correspondence with the SEM images. From the analysis of the color maps, the average ξ values were determined, according to a literature procedure.[29,30] For the samples deposited on the bare SiO_2 substrates, the ξ values were obtained considering only the areas where the P(DMS-*r*-VMS) cylinders are

clearly identified in the BCP films (Figure S4). The corresponding ξ values result approximately of 100 nm. In contrast, higher ξ values were observed when the surface was functionalized by grafting homopolymers or RCPs.

As reported in the previous section, the brush layers present nearly constant values in terms of thickness and roughness irrespective of their chemical composition. For this reason we expect that the lateral order of the BPC nanostructures ultimately depends on the interfacial energy between the brush layer and the BCP thin film. Figure 5 reports the average ξ values obtained from SEM analysis as a function of the WCA of the underlying substrate. Decreasing the WCA of the brush layer, the average ξ value progressively increases from 190 nm for the PS-*b*-P(DMS-*r*-VMS) film deposited on the P(S-*r*-MPDMS) brush layer to 260 nm for the one deposited on the PMMA brush layer.

It is interesting to note that the WCA measured on the PMMA brush layer is quite close to the one of the bare SiO_2 substrate. However, the morphology of the BCP thin films deposited on top of these two surfaces is significantly different in terms of homogeneity of the film and lateral order of the nanodomains. The origin of this difference is probably related to the distinct nature of the interfaces where the soft interface of the PMMA brush layer allows some interpenetration to occur whereas SiO_2 provides an hard and compact interface with little interaction available. Differences in the arrangement and lateral order of BCP thin films deposited on soft and hard interfaces were already reported.[45]

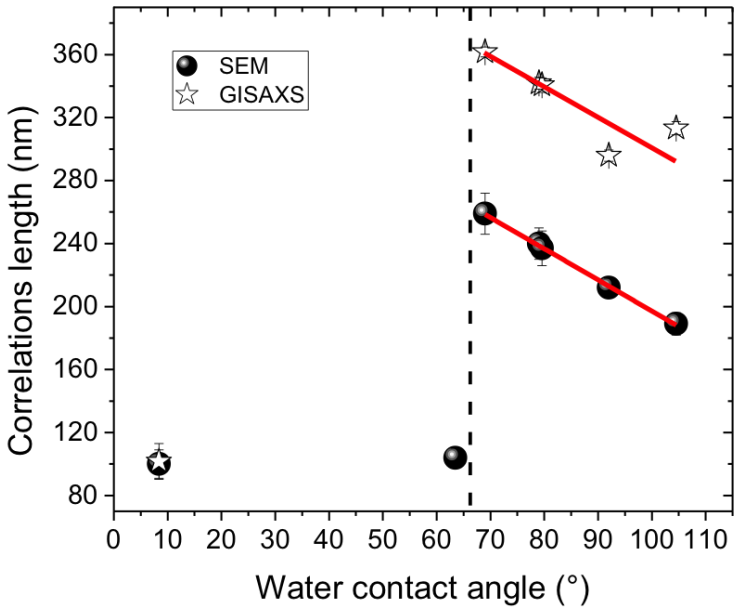

Figure 5. Correlations length ξ from SEM and GISAXS analysis as a function of the water contact angles of the substrates.

GISAXS measurements were performed to get additional structural data and validate the results obtained by elaboration of the SEM images. GISAXS technique provides information on the in-plane ordering of the cylindrical nanostructures, investigating a sample area orders of magnitude larger than the one inspected by typical SEM images. Moreover, when the angle of incidence exceeds the critical angle, GISAXS conveys information from the whole film thickness, thus providing a global (averaged) description of the sample. Representative GISAXS patterns are reported in Figure 6a for the PS-*b*-P(DMS-*r*-VMS) thin films on the different substrates. The components of the scattering vector normal and parallel to the plane of the sample are indicated as q_z and q_{xy}, respectively.

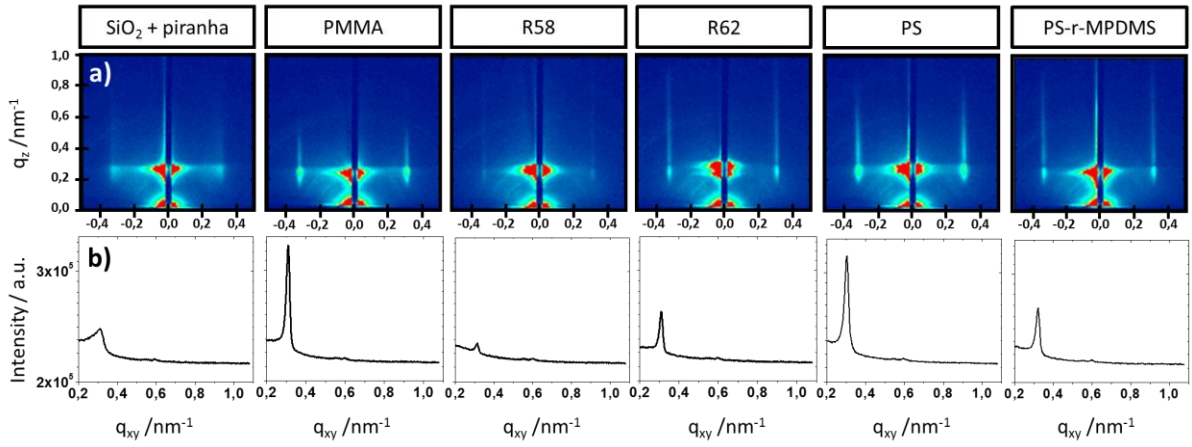

Figure 6. GISAXS patterns (rows a) and intensity profiles (row b) for PS-*b*-P(DMS-*r*-VMS) thin films on different substrates. All GISAXS patterns were recorded at an incident angle α_i = 0.19°. GISAXS intensity profiles are measured along q_{xy} at fixed q_z = 0.25 nm.

They were collected at an incident angle of 0.19°, above the BCP critical angle ($\alpha_c \approx 0.17°$ for the unetched PS-*b*-P(DMS-*r*-VMS) film, while it is significantly lower when PS is removed) but well below the SiO_2 and Si substrate critical angles at $\alpha_c \approx 0.25°$ and 0.26°, respectively. In this condition, the radiation penetration depth is much larger than the thickness of the BCP film. The sample on the as-received SiO_2 does not show any diffraction feature and is not reported in Figure 6. All other samples exhibit a pair of diffraction rods aligned along q_z. The absence of reflections in the out-of-plane direction indicates the presence of a single layer of cylinders.[46] The difference in the scattered intensity among the samples reflects a different in-plane modulation of refractive index and it is most probably related to a different degree of removal of the PS matrix. Compared to the others, the sample on piranha treated SiO_2 presents a broad and poorly defined diffraction peak, indicating a significantly lower degree of order.

Figure 6b shows the intensity profiles along q_{xy} obtained from horizontal cuts of the GISAXS patterns of Figure 6a at q_z = 0.25 nm^{-1}. The values of lattice spacing calculated from the q_{xy}

values corresponding to the peak maxima vary slightly from sample to sample, ranging between L_0 = 19.44 ± 0.07 nm and L_0 = 20.54 ± 0.08 nm for the samples on P(S-*r*-MPDMS) and on PS, respectively, in good agreement with those obtained from the statistical analysis of the SEM images. The width of the peaks provides a quantitative measure of the in-plane structural order. In general, one can quantify the degree of order through a correlation length parameter, ξ, inversely proportional to the full width at half maximum (FWHM) of the peak, Δq_{xy}, the proportionality constant being dependent on the model used to describe the structural order. Here we modeled the fingerprint structure of our samples as composed of randomly oriented grains where each grain consists of a set of perfectly ordered straight cylinders. The grain shape is assumed cylindrical with axis normal to the plane of the sample. The correlation length parameter, ξ, is defined as the average grain diameter, calculated by means of the classical Scherrer formula:[47]

$$\xi = K \frac{2\pi}{\Delta q_{xy}}$$

where K =1.03 is a constant related to the grain shape. Applying this model to the present data, the highest correlation length (ξ ~ 360 nm) is obtained for the PMMA brush layer and the lowest (ξ ~ 100 nm) for the sample spun on the piranha treated SiO_2 substrate.

The correlation lengths obtained from GISAXS data and those determined from SEM analysis are compared in Figure 5. The dependence of ξ on the WCA of the substrate is remarkably similar for the two sets of measurements, despite a difference exists in the absolute values. This discrepancy in the absolute values is not surprising, as determining a correlation length means to arbitrarily set a boundary in the transition between order and disorder, a process which is inherently continuous and spatially inhomogeneous. Accordingly, the values obtained with the

two distinct techniques are strongly dependent on the model-specific assumptions underlying each approach, making of little significance a direct comparison of the absolute values.

Temperature dependence of the correlation length

Once On the basis of the previous results, the PMMA grafted substrate was chosen to investigate evolution of ξ in PS-*b*-P(DMS-*r*-VMS) films as a function of T_a and t_a. To identify the upper limit of T_a, that allows promoting the self-assembly process without thermal degradation, the ordering was performed at temperatures ranging from 190 to 350 °C for the fixed t_a = 300 s.

Figure 7a shows a series of representative SEM plan view images taken at different T_a.

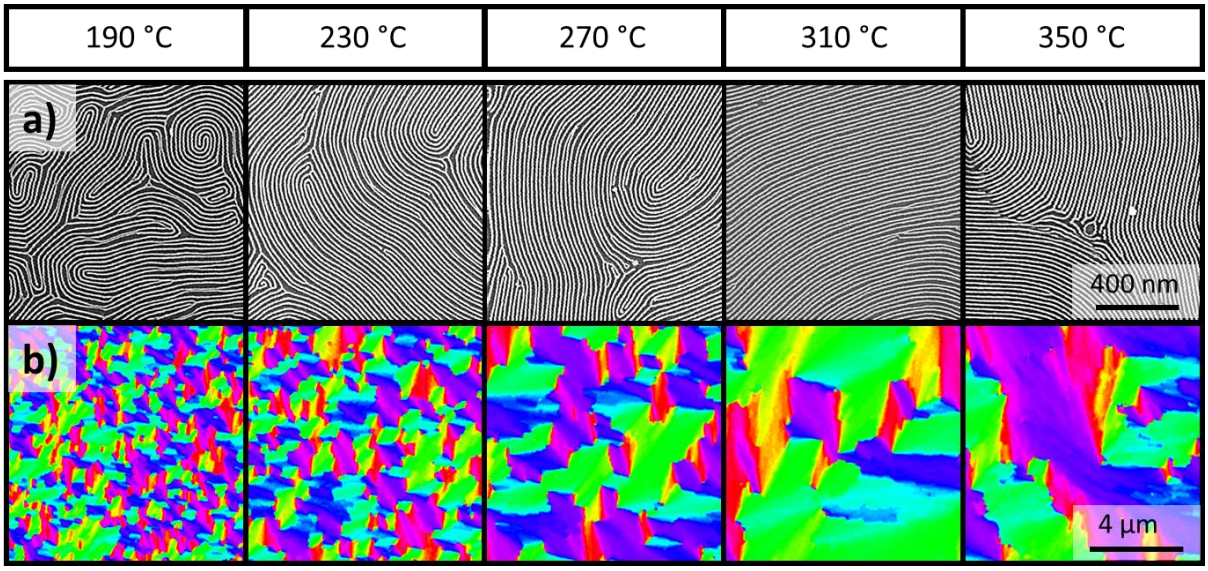

Figure 7. High magnification SEM images a) of the PS-*b*-P(DMS-*r*-VMS) thin films deposited on a PMMA brush layer and thermally treated at T_a = 190, 230, 270, 310, and 350 °C for t_a = 300 s. Color maps b), delimiting the domain boundaries, obtained from software analysis of the corresponding low magnification SEM images. The correlation between the color scale and the orientation of the cylinder in the polymeric film is reported in figure 4.

Corresponding to $T_a \leq 310$ °C, a perfectly homogeneous coverage of the surface was observed with P(DMS-*r*-VMS) cylinder parallel oriented with respect to the substrate. At $T_a > 310$ °C,

surface inhomogeneities appeared and their size progressively increased with temperature as shown in Figure 8b and 8c. In particular, the samples annealed at T_a = 330 °C exhibits small regions of the polymeric film characterized by different contrast (dark zone) in the SEM images. On further raising the temperature to 350 °C (Figure 8d and 8e), an increase in the size of the dark zones was detected. However, looking at these images in detail, a well-defined cylinder morphology was observed in the BCP film even in the dark zones, suggesting the different contrast in the SEM plan view images is related to a local thickness variation of the polymeric film. Tilted SEM images (figure S5) reveal that these dark zones effectively correspond to terraces. Considering that at this temperature the PS-*b*-P(DMS-*r*-VMS) is still quite stable, the origin of these dark regions has to be attributed to a degradation of the underlying brush layer of PMMA. In fact, the thermal stability of the PMMA employed in the surface grafting reaction revealed lower than that of the PS-*b*-P(DMS-*r*-VMS) (Figure S6). The same phenomenology was recently reported for PS-*b*-PMMA thin films ordered at high temperatures on a P(S-*r*-MMA) brush layer.[48]

The color maps extracted from the low magnification SEM images are reported in Figure 7b. The images indicate a progressive increase in the grain size when increasing T_a. Figure 8a shows the corresponding variation of ξ as a function of T_a. For the samples treated at 330 °C and 350 °C, ξ values were estimated in the portion of the samples where degradation is not visible. The correlation length increases with temperature, up to 1.65 μm, corresponding to T_a = 330 °C whereas, at T_a = 350 °C, a sudden decrease in ξ is observed.

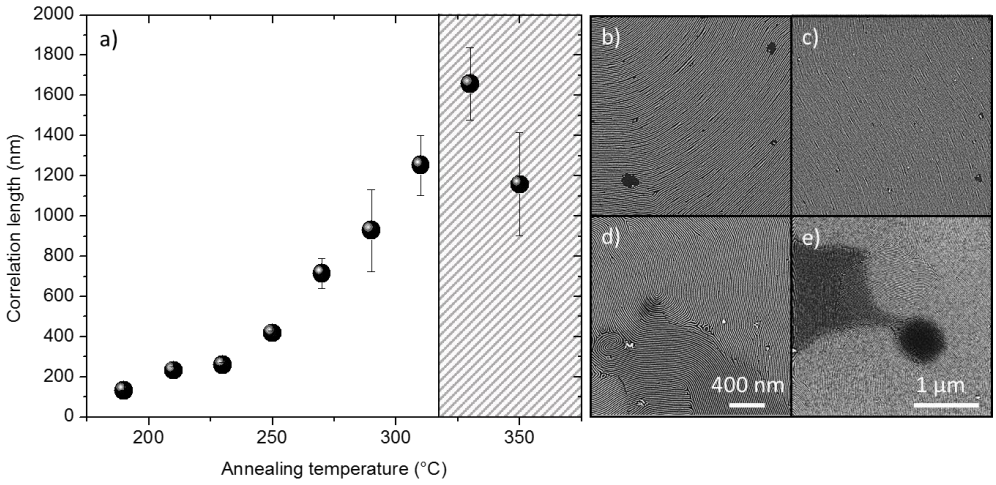

Figure 8. Temperature dependence of the PS-*b*-P(DMS-*r*-VMS) correlation length corresponding to t_a = 300 s (a).SEM images of the PS-*b*-P(DMS-*r*-VMS) thin films thermally treated at T_a = 330 °C (b), (c) and 350 °C (d), (e) for T_a = 300 s at high (left) and low (right) magnification.

Time dependence of the correlation length

According to the previous results, the maximum ξ was obtained annealing the samples at T_a = 330 °C. However, at this temperature, degradation of the PMMA grafted layer occurred, thus resulting in the appearance of dishomogeneous regions. On the other hand, after annealing at T_a = 310 °C for the same t_a = 300 s, the polymeric film did not show evidence of degradation and the corresponding ξ was only slightly lower than the one obtained at T_a = 330 °C. Accordingly, the time evolution of ξ at 310 °C could provide information about the kinetic of the lateral ordering process and the maximum achievable ξ value whilst maintaining a high level of homogeneity in the sample.

Figure 9 shows a collection of SEM plan view images and of the corresponding color maps taken at 310 °C after different t_a. The grain coarsening is clearly highlighted, indicating a growth of the nanodomains in the PS-*b*-P(DMS-*r*-VMS) thin films for $t_a \leq 300$ s.

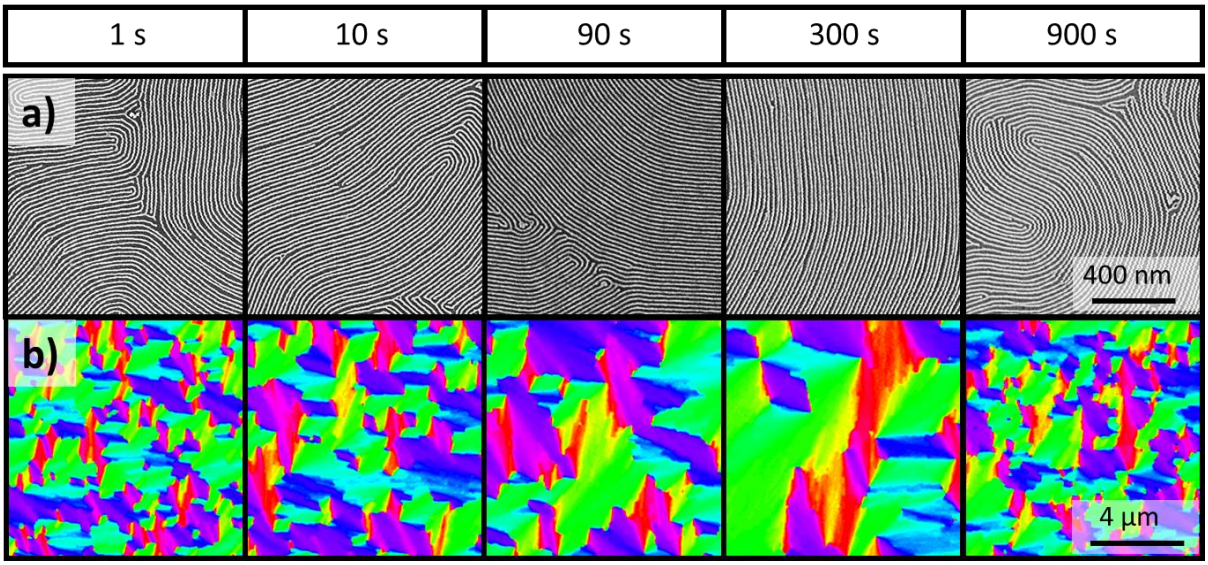

Figure 9. High magnification SEM plan view images of the PS-*b*-P(DMS-*r*-VMS) thin films annealed at T_a = 310 °C for different t_a (a) and color maps obtained by software analysis of the corresponding low magnification SEM images (b). The correlation between the color scale and the orientation of the cylinder in the polymeric film is reported in figure 4.

Figure 10a illustrates the trend of ξ as a function of t_a. The correlation length increases regularly with t_a up to 300 s according to a power law dependence $\xi(t) \approx t^{\phi}$ with the growth exponent ϕ = 0.21 ± 0.01. On further increasing t_a above 300 s, some dishomogeneous regions appear, as illustrated in Figure 10b and 10c, thus establishing the maximum achievable ξ value to about 1.25 µm.

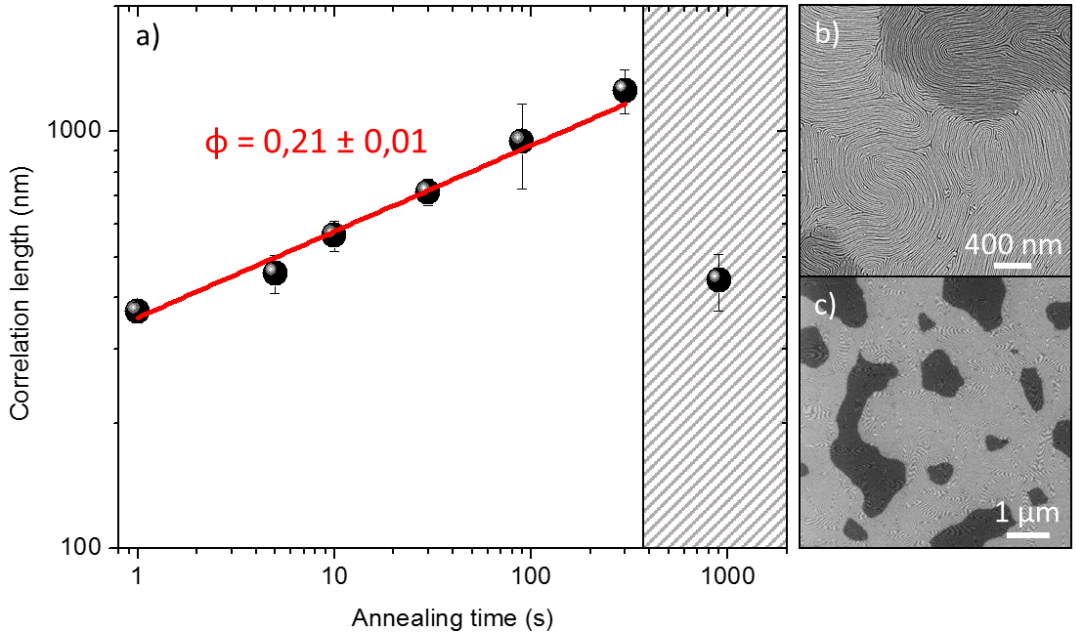

Figure 10. Evolution of the correlation length as a function of t_a in PS-*b*-P(DMS-*r*-VMS) thin films thermally treated in RTP at T_a = 310 °C (a). High magnification (b) and low magnification (c) SEM plan view images of PS-b-P(DMS-r-VMS) thin films in samples treated at T_a = 310 °C for t_a = 900 s.

DISCUSSION

The overall picture of the reported data demonstrates that PS-*b*-P(DMS-*r*-VMS) thin films provide a homogeneous coverage of the sample surface without any significant dewetting phenomenon, irrespective of the effective surface functionalization, thus allowing a systematic study of the lateral ordering evolution in PS-*b*-P(DMS-*r*-VMS) thin film as a function of the processing parameters.

The lateral order of parallel cylindrical P(DMS-*r*-VMS) nanostructures is affected by the surface nature of the substrate and the processing parameters (T_a, t_a). Hard surfaces are ineffective in

inducing long-range order. In contrast, soft interfaces are able to accommodate homogeneous PS-*b*-P(DMS-*r*-VMS) BCP films with high level of order in the polymeric template. Moreover the lateral order in the BCP film progressively increases reducing the WCA of the substrate. In particular it is worth to note that the correlation length ξ reaches a maximum value when the PS-*b*-P(DMS-*r*-VMS) film is deposited on top of a grafted PMMA layer. In principle PMMA is immiscible with PS and P(DMS-*r*-VMS) and consequently it is not expected to provide a suitable surface for the spinning and self-assembly of the PS-*b*-P(DMS-*r*-VMS) films. A clear understanding of this effect has not been achieved yet and further investigation are necessary to fully elucidate the effective interaction of the PS-*b*-P(DMS-*r*-VMS) BCP with the underlying substrate.

In terms of process parameters, two conflicting aspects should be taken into account for PS-*b*-P(DMA-*r*-VMS) films deposited on the PMMA brush layer. From one side, ξ increases as t_a and T_a increase. On the other side, the relative thermal instability of the grafted brush layer limits the development of the ordering process. Driving the sample to the final target temperature in a very short time, it is possible to promote the self-assembly and lateral ordering in the BCP thin film before the degradation of the grafted layer occurs. Consequently, fast heating rates are necessary to take advantage of the different time scale of the ordering and degradation processes. In this way, by properly adjusting both the surface nature of the substrate and the annealing parameters, correlation length values in the micrometer scale were obtained by a simple thermal treatment over the entire substrate without any additional external stimuli. Few minute processing time in RTP was required to achieve long-range order in the BCP thin films.

The extension of this approach to other silicon containing BCP is not straightforward since it is strictly related to the capability to achieve uniform coverage of the substrates and to avoid

thermal degradation of the specific silicon containing block. From a general point of view, we observe that the RTP treatment efficiently promotes the self-assembly in PS-*b*-P(DMS-*r*-VMS) thin films, achieving a level of lateral ordering that is better than, or at least comparable to the ones obtained in PS-*b*-PDMS thin films with more complex processing approaches.[23,37] An accurate comparison with the data reported in the literature is not clear-cut. Indeed in many papers the level of order is demonstrated through the qualitative comparison of SEM images, without any systematic assessment of the lateral order trough a quantitative measurement of the ξ values.

In this regard it is interesting to note that the measurement of the correlation length does not provide a complete description of pattern quality in the self-assembled material over large areas of the sample. Defectivity of the polymeric templates within the nanodomains represents an important issue in order to effectively introduce these materials into lithographic processes.[49] However, the analysis of the evolution of the correlation length as a function of the processing parameters provides a first quantitative indication of the kinetics of lateral ordering and grain coarsening in the polymeric template. As already discussed, no systematic and quantitative data about the lateral order evolution in silicon-containing BCP thin films are available. The qualitative analysis of the SEM images reported in the literature indicates that, irrespective of N values, very poor levels of order were achieved in silicon-containing BCPs by simple thermal treatments without the introduction of external guiding fields.[18,19,50] Conversely, several papers provide data about the evolution of lateral order in low-χ cylinder forming BCP thin films with nanodomains parallel oriented with respect to the substrate. Since the assembly kinetics is strictly related to the χN value,[51,52] it is interesting to compare the evolution of ξ observed in our PS-*b*-P(DMS-*r*-VMS) thin films treated at 310 °C with those of low-χ cylinder forming BCP with

similar χN values. In particular, detailed investigations of the grain coarsening process are reported for low-χ PS-*b*-PB;[29] PS-*b*-PI;[53] PS-*b*-PMMA[54] BCPs with χ*N* values around 20 at ~ 200 °C. This χN value is very close to the one we calculated for the PS-*b*-P(DMS-*r*-VMS) BCP treated at 310 °C. For all these low-χ BCPs, the evolution ξ(t) of the correlation length as a function of the annealing time exhibits a power law dependence with growth exponent ϕ ~ 0.25. Within the experimental error, this value is very close to the growth exponent we measured in the PS-b-P(DMS-r-VMS) thin films suggesting that the ordering evolution in the PS-*b*-P(DMS-*r*-VMS) films follows the same dynamics reported for several low-χ block copolymers.[29,53,54] This result was obtained using a standard thermal treatment at high temperature, without introducing any specifically designed set-up for the processing of the BCP thin films. The possibility to operate with a very simple set up and the short annealing time required to promote long range ordering in the polymeric template indicate PS-*b*-P(DMS-*r*-VMS) as a suitable candidate for the integration in the lithographic process flow of an industrial production line.

From a technological point of view, the possibility to achieve the perpendicular orientation of the cylindrical nanodomainsin silicon containing BCP thin films would be extremely interesting. The achievement of this goal is very challenging, because the difference in the surface-free energy between the two blocks is very high, inducing preferential wetting of the siloxane component at the free surface of the BCP thin film. Recently Bates *et al.*,[55] Durand *et al.*,[56] and Maher *et al.*,[57,58] obtained the perpendicular orientation of the nanodomains in silicon containing BCP thin films during a thermal treatment by means of switching-polarity top-coat control methods. Alternatively Aissou *et al.*[24] reported that perpendicular orientation of cylinder in polycarbosilane-based BCP can be obtained within a topographically defined guiding pattern by thermal annealing. Very recently Seshimoto *et al.*[25] obtained perpendicular oriented lamellar

structures in thin films of polysiloxane-based BCPs by means of a simple thermal treatment without the introduction of external guiding structures or top-coats. The authors introduced hydroxyl groups in the modified polysiloxane block of a PS-b-PMVS, exploiting the vinyl groups in the side chain of the polysiloxane block. The introduction of the hydroxyl groups allows properly balancing the surface free energy of the polysiloxane and polystyrene blocks at the air interface, preventing preferential wetting of one of the two blocks and consequently leading to perpendicular orientation of the cylinders with respect to the substrate. The application of this approach to our silicon-containing BCP would allows achieving perpendicular orientation of the nanodomains and long range order within the polymeric film with a simple RTP treatment in a short processing time.

CONCLUSIONS

In conclusion, by properly tuning the processing parameters, a simple thermal treatment in a RTP machine was effective to promote the self-assembly of cylindrical P(DMS-*r*-VMS) nanostructures parallel to the substrate in PS-*b*-P(DMS-*r*-VMS) thin films. Using a PMMA brush layer, it was possible to guarantee a uniform coverage of the substrate. Moreover, operating at high temperature (310 °C, 300 s), long-range order of the nanodomains was achieved without any evidence of degradation in the BCP film. Correlation length values of 1.25 μm were obtained on flat substrates without any external field to induce directional alignment. This work demonstrates that high temperature processing of this high-χ copolymer is possible and allows overcoming the limitations related to the low diffusivity of the PS-*b*-P(DMS-*r*-VMS) polymeric chains, delineating a strategy for the integration of these self-assembling materials in conventional lithographic processes.

AUTHOR INFORMATION

Corresponding author

*E-mail: tommaso.giammaria@mdm.imm.cnr.it; michele.perego@mdm.imm.cnr.it; michele.laus@uniupo.it

ASSOCIATED CONTENT

Supporting Information.

Merging between color map and the corresponding SEM image, AFM images of the polymer brushes; cross-sectional SEM image of the cylindrical nanostructures parallel oriented with respect to the substrate; SEM images of silicon nanostructures on SiO_2 and piranha treated SiO_2 substrates; tilted SEM image of the dark zone; comparison among the integral of DEP-MS signals for PMMA and PS-*b*-P(DMS-*r*-VMS).

This material is available free of charge via the Internet at http://pubs.acs.org.

ACKNOWLEDGMENT

The authors acknowledge Jean-Sebastien Micha (ESRF) for technical support in the GISAXS measurements and Dr. Jacopo Frascaroli (IMM-CNR) for AFM analysis. This research activity was partially funded by the European Metrology Research Programme (EMRP), project new01-TReND. The EMRP is jointly funded by the EMRP participating countries within EURAMET and the European Union. Partial financial support by PRIN 2010-2014 "Materiali Polimerici Nanostrutturati con Strutture Molecolari e Cristalline Mirate" is acknowledged. Patent protection related to this work is pending.

REFERENCES

(1) Sanders, D. P. Advances in Patterning Materials for 193 Nm Immersion Lithography. *Chem. Rev.* **2010**, *110*, 321–360.

(2) Bang, J.; Jeong, U.; Ryu, D. Y.; Russell, T. P.; Hawker, C. J. Block Copolymer Nanolithography: Translation of Molecular Level Control to Nanoscale Patterns. *Adv. Mater.* **2009**, *21*, 4769–4792.

(3) The International Technology Roadmap for Semiconductors (ITRS), "Emerging Research Materials," 2007.

(4) Hamley, I. W. Ordering in Thin Films of Block Copolymers: Fundamentals to Potential Applications. *Prog. Polym. Sci.* **2009**, *34*, 1161–1210.

(5) Darling, S. B. Directing the Self-Assembly of Block Copolymers. *Prog. Polym. Sci.* **2007**, *32*, 1152–1204.

(6) Bates, C. M.; Maher, M. J.; Janes, D. W.; Ellison, C. J.; Willson, C. G. Block Copolymer Lithography. *Macromolecules* **2014**, *47*, 2–12.

(7) Ahn, H.; Ryu, D. Y.; Kim, Y.; Kwon, K. W.; Lee, J.; Cho, J. Phase Behavior of Polystyrene- B -Poly(methyl Methacrylate) Diblock Copolymer. *Macromolecules* **2009**, *42*, 7897–7902.

(8) Russell, T. P.; Hjelm, R. P.; Seeger, P. A. Temperature Dependence of the Interaction Parameter of Polystyrene and Poly (methy1 Methacrylate). *Macromolecules* **1990**, *23*, 890–893.

(9) Seguini, G.; Giammaria, T. J.; Lupi, F. F.; Sparnacci, K.; Antonioli, D.; Gianotti, V.; Vita, F.; Placentino, I. F.; Hilhorst, J.; Ferrero, C.; Francescangeli, O.; Laus, M.; Perego, M. Thermally Induced Self-Assembly of Cylindrical Nanodomains in Low Molecular Weight PS-B-PMMA Thin Films. *Nanotechnology* **2014**, *25*, 045301.

(10) Luo, M.; Epps, T.H. Directed Block Copolymer Thin Film Self-Assembly: Emerging Trends in Nanopattern Fabrication. *Macromolecules* **2013**, *46*, 7567–7579.

(11) Nose, T. Coexistence Curves of Polystyrene/Poly(dimethylsiloxane) Blends. *Polymer* **1995**, *36*, 2243–2248.

(12) Son, J.G.; Chang, J.B.; Berggren, K.K.; Ross, C.A. Assembly of Sub-10-nm Block Copolymer Patterns with Mixed Morphology and Period Using Electron Irradiation and Solvent Annealing. *Nano Lett.* **2011**, *11*, 5079–5084.

(13) Gotrik, K.W.; Hannon, A.F.; Son, J.G.; Keller, B.; Alexander-Katz, A.; Ross, C.A. Morphology Control in Block Copolymer Films Using Mixed Solvent Vapors. *ACS Nano* **2012**, *6*, 8052–8059.

(14) Son, J.G.; Gotrik, K.W.; Ross, C.A. High-Aspect-Ratio Perpendicular Orientation of PS-b-PDMS Thin Films under Solvent Annealing. *ACS Macro Lett.* **2012**, *1*, 1279–1284.

(15) Kim, J.M.; Kim, Y.J.; Park, W.I.; Hur, Y.H.; Jeong, J.W.; Sim, D.M.; Baek, K.M.; Lee, J.H.; Kim,M.J.; Jung, Y.S. Eliminating the Trade-Off between the Throughput and Pattern Quality of Sub-15 nm Directed Self-Assembly via Warm Solvent Annealing. *Adv. Func. Mat.* **2014**, 25, 306–315.

(16) Deshpande, G.; Rezac, M.E. Kinetic Aspects of the Thermal Degradation of Poly(Dimethyl Siloxane) and Poly(Dimethyl Diphenyl Siloxane). *Polym. Degrad. Stab.* **2002**, *76*, 17–24.

(17) Sinturel, C.; Vayer, M.; Morris, M.; Hillmyer, M. Solvent Vapor Annealing of Block Polymer Thin Films. *Macromolecules* **2013**, *46*, 5399–5415.

(18) Park, W.I.; Tong, S.; Liu, Y.; Jung, I.W.; Roelofs, A.; Hong, S. Tunable and Rapid Self-Assembly of Block Copolymers Using Mixed Solvent Vapors. *Nanoscale* **2014**, *6*, 15216–15221.

(19) Park, W. I.; Kim, K.; Jang, H.I.; Jeong, J.W.; Kim, J.M.; Choi, J.; Park, J.H.; Jung, Y.S. Directed Self-Assembly with Sub-100 Degrees Celsius Processing Temperature, Sub-10 Nanometer Resolution, and Sub-1 Minute Assembly Time. *Small* **2012**, *8*, 3762–3768.

(20) Rasappa, S.; Schulte, L.; Borah, D.; Morris, M.A.; Ndoni, S. Rapid, Brushless Self-Assembly of a PS-B-PDMS Block Copolymer for Nanolithography. *Colloids Interface Sci. Commun.* **2014**, *2*, 1–5.

(21) Zhang, X.; Harris, K.D.; Wu, N.L.Y.; Murphy, J.N.; Buriak, J. M. Fast Assembly of Ordered Block Microwave Annealing. *ACS Nano* **2010**, *4*, 7021–7029.

(22) Jin, C.; Murphy, J.N.; Harris, K.D.; Buriak, J.M. Deconvoluting the Mechanism of Microwave Annealing of Block Copolymer Thin Films. *ACS Nano* **2014**, *8*, 3979–3991.

(23) Yoon, E.; Kim, E.; Kim, D.; Son, J.G. Top-Coat Dewetting for the Highly Ordered Lateral Alignment of Block Copolymer Microdomains in Thin Films. *Adv. Funct. Mater.* **2015**, *25*, 913–919.

(24) Aissou, K.; Mumtaz, M.; Fleury, G.; Portale, G.; Navarro, C.; Cloutet, E.; Brochon, C.; Ross, C.A.; Hadziioannou, G. Sub-10 nm Features Obtained from Directed Self-Assembly of Semicrystalline Polycarbosilane-Based Block Copolymer Thin Films. *Adv. Mater.* **2015**, 27, 261–265.

(25) Seshimo, T.; Maeda, R.; Odashima, R.; Takenaka, Y.; Kawana, D.; Ohmori, K.; Hayakawa, T. Perpendicularly Oriented Sub-10 nm Block Copolymer Lamellae by Atmospheric Thermal Annealing for One Minute. *Sci. Rep*. **2016**, 6, 19481, doi: 10.1038/srep19481.

(26) Sparnacci, K.; Antonioli, D.; Gianotti, V.; Laus, M.; Zuccheri, G.; Ferrarese Lupi, F.; Giammaria, T.J.; Seguini, G.; Ceresoli, M.; Perego, M. Thermal Stability of Functional P(S-R-MMA) Random Copolymers for Nanolithographic Applications. *ACS Appl. Mater. Interfaces* **2015**, *7*, 3920–3930.

(27) Jakubowski, W.; Min, K.; Matyjaszewski, K. Activators Regenerated by Electron Transfer for Atom Transfer Radical Polymerization of Styrene. *Macromolecules* **2006**, *39*, 39–45.

(28) Ferrarese Lupi, F.; Giammaria, T J.; Ceresoli, M.; Seguini, G.; Sparnacci, K.; Antonioli, D.; Gianotti, V.; Laus, M.; Perego, M. Rapid Thermal Processing of Self-Assembling Block Copolymer Thin Films. *Nanotechnology* **2013**, *24*, 315601.

(29) Harrison, C.; Chaikin, P.M.; Huse, D.A.; Register, R.A.; Adamson, D.H.; Daniel, A.; Huang, E.; Mansky, P.; Russell, T.P.; Hawker, C.J.; Egolf, D.A.; Melnikov, I.V.; Bodenschatz, E. Reducing Substrate Pinning of Block Copolymer Microdomains with a Buffer Layer of Polymer Brushes. *Macromolecules* **2000**, *33*, 857–865.

(30) Ceresoli, M.; Volpe, F.G.; Seguini, G.; Antonioli, D.; Gianotti, V.; Sparnacci, K.; Laus, M.; Perego, M. Scaling of Correlation Length in Lamellae Forming PS-b-PMMA Thin Films Upon High Temperature Rapid Thermal Treatments. *J. Mater. Chem. C* **2015**, 3, 8618-8624.

(31) Gianotti, V.; Antonioli, D.; Sparnacci, K.; Laus, M.; Giammaria, T.J.; Ceresoli, M.; Ferrarese Lupi, F.; Seguini, G.; Perego, M. Characterization of Ultra-Thin Polymeric Films by Gas Chromatography-Mass Spectrometry Hyphenated to Thermogravimetry. *J. Chromatogr. A* **2014**, *1368*, 204–210.

(32) Faravelli, T.; Pinciroli, M.; Pisano, F.; Bozzano, G.; Dente, M.; Ranzi, E. Thermal Degradation of Polystyrene. *J. Anal. Appl. Pyrolysis* **2001**, *60*, 103–121.

(33) Gianotti, V.; Antonioli, D.; Sparnacci, K.; Laus, M.; Giammaria, T.J.; Ferrarese Lupi, F.; Seguini, G.; Perego, M. On the Thermal Stability of PS-b-PMMA Block and PS-R-PMMA Random Copolymers for Nanopatterning Applications. *Macromolecules* **2013**, *46*, 8224–8234.

(34) Welander, A.M.; Kang, H.; Stuen, K.O.; Solak, H.H.; Müller, M.; de Pablo, J.J.; Nealey, P.F. Rapid Directed Assembly of Block Copolymer Films at Elevated Temperatures. *Macromolecules* **2008**, 41, 2759-2761.

(35) Manring, L.E. Thermal Degradation of Poly(methyl methacrylate). 2. Vinyl-terminated Polymer. *Macromolecules* **1989**, 22, 2673-2677

(36) Perego, M.; Ferrarese Lupi, F.; Ceresoli, M.; Giammaria, T.J.; Seguini, G.; Enrico, E.; Boarino, L.; Antonioli, D.; Gianotti, V.; Sparnacci, K.; Laus, M. Ordering Dynamics in Symmetric PS-B-PMMA Diblock Copolymer Thin Films During Rapid Thermal Processing. *J. Mater. Chem. C* **2014**, *2*, 6655–6664.

(37) Borah, D.; Rasappa, S.; Senthamaraikannan, R.; Kosmala, B.; Shaw, M.T.; Holmes, J.D.; Morris, M.A. Orientation and Alignment Control of Microphase-Separated PS-b-PDMS Substrate Patterns via Polymer Brush Chemistry. *ACS Appl. Mater. Interfaces* **2013**, 5, 88-97.

(38) Jung, Y.S.; Ross, C. Orientation-Controlled Self-Assembled Nanolithography Using a Polystyrene - Polydimethylsiloxane Block Copolymer. *Nano Lett.* **2007**, *7*, 2046–2050.

(39) Xiao, S.; Yang X.M.; Park, S.; Weller, D.; Russell, T.P. A Novel Approach to Addressable 4 Teradot/in.^{2} Patterned Media. *Adv. Mater.* **2009**, 21, 2516-2519

(40) Benjamin, M.D.; O'Driscoll; Roisin, A.K., Shaw, M.; Mokarian-Tabari, P.; Liontos, G.; Ntetsikas, K.; Avgeropoulos, A.; Petkov, N.; Morris, M.A. *European Polymer Journal* **2013**, 49, 3445-3454.

(41) Ferrarese Lupi, F.; Giammaria, T.J.; Seguini, G.; Ceresoli, M.; Perego, M.; Antonioli, D.; Gianotti, V.; Sparnacci, K.; Laus, M. Flash Grafting of Functional Random Copolymers for Surface Neutralization. *J. Mater. Chem. C* **2014**, *2*, 4909–4917.

(42) Iyer, K.S.; Luzinov, I. Effect of Macromolecular Anchoring Layer Thickness and Molecular Weight on Polymer Grafting. *Macromolecules* **2004**, *37*, 9538–9545.

(43) Hexemer, A.; Stein, G.E.; Kramer, E.J.; Magonov, S. Block Copolymer Monolayer Structure Measured with Scanning Force Microscopy Moiré Patterns. *Macromolecules* **2005**, *38*, 7083–7089.

(44) Borah, D.; Shaw, M.T.; Holmes, J.D.; Morris, M.A. Sub-10 Nm Feature Size PS-B-PDMS Block Copolymer Structures Fabricated by a Microwave-Assisted Solvothermal Process. *ACS Appl. Mater. Interfaces* **2013**, *5*, 2004–2012.

(45) Xu, T.; Kim, H.; DeRouchey, J.; Seney, C. The Influence of Molecular Weight on Nanoporous Polymer Films. *Polymer* **2001**, *42*, 9091–9095.

(46) Qiang, Z.; Zhang, L.; Stein, G.E.; Cavicchi, K.A.; Vogt, B.D. Unidirectional Alignment of Block Copolymer Films Induced by Expansion of a Permeable Elastomer during Solvent Vapor Annealing. *Macromolecules* **2014**, *47*, 1109–1116.

(47) Smilgies, D.M. Scherrer Grain-Size Analysis Adapted to Grazing-Incidence Scattering with Area Detectors. *J. Appl. Crystallogr.* **2009**, *42*, 1030–1034.

(48) Ceresoli, M.; Lupi Ferrarese, F.; Seguini, G.; Sparnacci, K.; Gianotti, V.; Antonioli, D.; Laus, M.; Boarino, L.; Perego, M. Evolution of Lateral Ordering in Symmetric Block

Copolymer Thin Films upon Rapid Thermal Processing. *Nanotechnology* **2014**, *25*, 275601.

(49) Li, W.; Mueller, M. Defects in the Self-Assembly of Block Copolymers and Their Relevance for Directed Self-Assembly. *Annu. Rev. Chem. Biomol. Eng.* **2015**, 6, 187-216.

(50) Jeong, J.W.; Park, W.I.; Kim, M.J.; Ross, C.A.; Jung, Y.S. Highly Tunable Self-Assembled Nanostructures from a Poly(2-Vinylpyridine-b-Dimethylsiloxane) Block Copolymer. *Nano Lett.* **2011**, *11*, 4095–4101.

(51) Yokoyama, H.; Kramer, J.E. Diffusion of Triblock Copolymers in a Spherical Domain Structure. *Macromolecules* **2000**, 33, 954-959.

(52) Lodge, T.P.; Dalvi, M.C. Mechanisms of Chain Diffusion in Lamellar Block Copolymers. *Phys. Rev. Lett.* **1995**, 75, 657-660.

(53) Harrison, C.; Adamson, D.H.; Cheng, Z.; Sebastian, J.M.; Sethuraman, S.; Huse, D.A.; Register, R.A.; Chaikin, P.M. Mechanisms of Ordering in Striped Patterns. *Science* **2000**, *290*, 1558–1560.

(54) Ruiz, R.; Bosworth, J.K.; Black, C.T. Effect of Structural Anisotropy on the Coarsening Kinetics of Diblock Copolymer Striped Patterns. *Phys. Rev. B* **2008**, *77*, 054204.

(55) Bates, C.M.; Seshimo, T.; Maher, T.M.; Durand, W.J.; Cushen, J.D.; Dean, L.M.; Blachut, G.; Ellison, C.J.; Willson, C.G. Polarity-Switching Top Coats Enable Orientation of Sub–10 nm Block Copolymer Domains. *Science* **2012**, 338, 775-779.

(56) Durand, W.J.; Blachut, G.; Maher, M.J.; Sirard, S.; Tein, S.; Carlson, M.C.; Asano, Y.; Zhou, S.X.; Lane, A.P.; Bates, C.M.; Ellison, C.J.; Willson, C.G. Design of High-χ Block Copolymers for Lithography. *J. Polym. Sci. A* **2015**, 53, 344-352.

(57) Maher, M.J.; Rettner, C.T.; Bates, C.M.; Blachut, G.; Carlson, M.C.; Durand, W.J.; Ellison, C.J.; Sanders, D.P.; Cheng, J.Y.; Willson, C.G. Directed Self-Assembly of Silicon-Containing Block Copolymer Thin Films. *ACS Appl. Mater. Interfaces* **2015**, 7, 3323-3328.

(58) Maher, M.J.; Bates, C.M.; Blachut, Sirard, G.S.; Self, J.L.; Carlson, M.C.; Dean, L.M.; Cushen, J.D.; Durand, W.J.; Hayes, C.O.; Ellison, C.J.;Willson, C.G. Interfacial Design for Block Copolymer Thin Films. 2014, *Chem. Mater.* **2014**, 26, 1471-1479.